Evidence for Rainfall-Triggered Earthquake Activity

Sebastian Hainzl[1], **Toni Kraft**[2], **Joachim Wassermann**[2], **Heiner Igel**[2] **and Eberhard Schmedes**[2]

[1] Institute of Geosciences, University of Potsdam, Postfach 60 15 53, D-14415 Potsdam, Germany; Email: hainzl@geo.uni-potsdam.de

[2] Department of Earth and Environmental Sciences, Geophysics Section, Ludwig-Maximilians-University, Theresienstr. 41, 80333 Munich, Germany

Evidence for Rainfall-Triggered Earthquake Activity

Sebastian Hainzl[1], Toni Kraft[2], Joachim Wassermann[2], Heiner Igel[2], Eberhard Schmedes[2]

The Earth's crust is known to be rather unstable. However, here we show that the crust can be so unstable that even very tiny pressure variations associated with precipitation trigger earthquakes in a few kilometer depth. Based on the observations of the isolated seismicity below the densely monitored Mt. Hochstaufen, SE Germany, we demonstrate that the spatiotemporal pore pressure changes due to diffusing rain water are highly correlated with the recorded seismicity and that the seismicity rate is well described by rate-state frictional response of faults. Our results indicate that a few millibar stress increase are enough to trigger earthquakes.

In recent years, hydromechanical coupling has been proposed as a possible explanation for many geological phenomena including the anomalous weakness of many major faults (*1*), silent slip events (*2*), aftershocks occurrence (*3, 4*), and

remote triggering of earthquakes (*5*). The widely accepted understanding is that an increase of the pore fluid pressure reduces the effective normal stress and thus the strength of faults, promoting earthquake rupture. Direct evidence for fluids affecting the stability of faults comes from reservoir induced seismicity (*6*), and fluid injections in wells (*7*) where induced pore pressure changes are high. Pressure variations associated with precipitation are commonly expected to be too tiny to affect earthquake initiation. Based on our observations for the isolated seismicity below the Mt. Hochstaufen, we are now able to show that rainfall can trigger earthquakes via the mechanism of fluid diffusion.

The Staufen Massif is an east-west striking mountain chain in SE Germany, northwest of the town Bad Reichenhall. The most prominent summit, Mt. Hochstaufen, reaches an altitude of 1775m (Fig. 1). Belonging to the elongated fold-and-thrust belt of the Northern Limestone Alps, the geology of the Staufen Massif is dominated by lower to middle Triassic limestone and dolomite (*10*). Since more than 600 years ago, earthquakes with maximum macroseismic intensities of I_0 = V have been reported in this region, which is embedded in an almost quiet surrounding. The majority of the earthquakes occurs in the summer months, which are also characterized by having the highest average precipitation values during the year (*11*). To explore the underlying mechanisms, seismic monitoring of the Bad Re-

ichenhall area was initiated in 2001, consisting of six permanent and three mobile short period stations (see locations in Fig. 1). In 2002, this network recorded more than 1100 earthquakes with a maximum magnitude of $M_l = 2.4$, mainly concentrated in two swarm type sequences following above-average rainfall in March and August. For the first time, these data allow a detailed analysis of the activity in this rare example of an isolated but critical system.

The observed seismicity is inconspicuous in its magnitude-frequency distribution that follows the Gutenberg-Richter law with a typical b-value of 1.1$\pm$0.1 for magnitudes larger than M_l=-0.2. Below this value the distribution deviates from the Gutenberg-Richter law, indicating incomplete data collection. We therefore restrict our analysis to $M_l \geq -0.2$ events. Hypocenter locations are derived for a subset of these events using a 2D-velocity model with topography. Groups of events with very similar wave forms are identified by cluster analysis and relocated using the master event technique (*12*). In this way, over 500 locations were obtained, shown as points in Fig. 1.

In order to test the hypothesis that rainfall triggered seismicity, we calculate the pore-fluid pressure changes at depth in response to the surface rain under the assumption of a source free, homogeneous half space, with scalar hydraulic diffusivity D. Following the theory of poroelasticity (*13*), the low frequency evolution

of pore pressure p due to irrotational flow can then be described by the diffusion equation (*14*), $\dot{p} = D\triangle p$. The solution for the one dimensional pore pressure diffusion driven by a source $P_0(t)$ at z=0 is given by (*15*)

$$p(z,t) = \int_{-\infty}^{t} G(z,t-\tau)P_0(\tau)d\tau \quad (1)$$

with Green's function $G(z,t-\tau) = [4\pi D(t-\tau)]^{-0.5}\exp[-z^2/4D(t-\tau)]$. In our case, the source is the linearly interpolated rain rate which is measured at four daily sampled meteorologic stations surrounding Mt. Hochstaufen. The location of our source at the free surface is taken care of by doubling the amplitude of the Green's function. Because we are only interested in pressure changes, we consider the deviation of the rainfall from the long-term mean, namely $P_0(t) = \rho g(h(t)-\bar{h})$. The average rain amount $\bar{h}$ is calculated from the precipitation data from 1995-2001 at the same meteorological stations. To avoid boundary effects, we start the integration of Eq.(1) at 1/1/2001.

To quantify the effect of the pressure changes on seismicity, we use the framework of rate-state friction (*8, 9*) which properly takes into consideration the rate- and slip-dependence of frictional strength and time-dependent restrengthening observed in laboratory experiments. This concept has already been successfully applied to explain earthquake clustering in nature such as aftershock activity (*16*). In this theory, the seismicity rate λ is inversely proportional to the state variable

γ describing the creep velocities on the faults, namely $\lambda(z,t) = \lambda_0/(\dot{\tau}\gamma(z,t))$, where λ_0 is the stationary background rate and $\dot{\tau}$ the tectonic loading rate. The evolution of the state variable can be tracked for arbitrary stressing histories by breaking the loading history into a discrete series of sufficiently small stress steps (*8*, *9*). In our case, the Coulomb failure stress (*17*) (CFS) changes due to the variation of the pore pressure p, altering the effective normal stress $\sigma = \sigma_n - p$ on the faults. Thus the stress steps are $\triangle CFS(z,t) = \mu(p(z,t+\triangle t) - p(z,t))$ where the coefficient of friction μ is set to the typical value (*18*) of 0.6 and the step size $\triangle t$ is 0.5 days. We track the state variable by iterating

$$\dot{\tau}\gamma(z,t+\triangle t) = (\tilde{\gamma}-1)\, e^{-\frac{\triangle t}{t_a}} + 1 \quad (2)$$

$$\text{with} \quad \tilde{\gamma} = \dot{\tau}\gamma(z,t)\, e^{\frac{-\triangle CFS}{A\sigma}} \quad (3)$$

starting from the background level, that is, $\dot{\tau}\gamma(z,0) = 1$. Because the pressure changes are assumed to be much smaller than the effective normal stress, we can use $A\sigma$ as a constant free parameter. The rate depends additionally on the value of the background rate λ_0, the relaxation time $t_a = A\sigma/\dot{\tau}$, and implicitly on the hydraulic diffusivity D.

The estimation of the four parameters is carried out by the maximum likelihood method. The log-likelihood with respect to the N earthquakes occurring at

the depth interval $[z_o, z_1]$ at times t_i is given by

$$\ln L(\lambda_0, t_a, A\sigma, D) = \sum_{i=1}^{N} \ln \lambda(z_i, t_i) - \int_{t_s}^{t_e} \int_{z_0}^{z_1} \lambda(z,t) dz dt \ , \qquad (4)$$

where t_s=1/1/2002 is the starting and t_e=1/1/2003 the ending time of the activity (*19*). We account for the uncertainty of earthquake locations by evaluating the formula (4) for z_i which are Gaussian distributed around the determined values. According to the localization procedure, the location errors vary between $50m$ and $2km$ with a median of $200m$.

For the earthquakes in the depth interval 1-4 km, the maximization of the likelihood function (Eq. 4) yields λ_0=0.45$\pm$0.05 [$days^{-1}$], t_a=150$\pm$40 [$days$], $A\sigma$=0.0011$\pm$0.0001 [bar] and a hydraulic diffusivity D= 0.25$\pm$0.05 $km^2/day \approx$ 2.9$\pm$0.6 m^2/s. The resulting diffusivity value corresponds well to results obtained from fluid injection experiments (*14*). Using the estimated value for hydraulic diffusivity, we calculate the pore pressure variations at depth from the observed rainfall (Fig.2a). The comparison of the observed seismic activity with the resulting spatio-temporal pressure field is shown in Fig.2b and with the forecasted earthquake rate in Fig.2c. In either case, the observed seismicity (indicated by stars) corresponds well to elevated values of the calculated functions, indicating a strong spatial and temporal correlation. In Fig.2d, the calculated and observed earthquake rate, including also the events without hypocentre in-

formation ($M_l \geq -0.2$), are compared in the form of time series representing the number of earthquakes per day. The correlation between these time series and between those of observed earthquake rate and rainfall is quantified by their cross-correlation coefficient, shown in Fig. 3. While the seismicity is not correlated with the rain data at zero time delay, it shows some correlation if the seismicity is shifted backwards 8 days (R_{max}=0.47). On the other hand, the earthquake rate calculated from the pore pressure changes at depth is strongly correlated at zero delay time with a maximum correlation coefficient, almost doubling that of the rain data (R_{max}=0.82). Note that the value of the hydraulic diffusivity that maximizes the likelihood function in Eq. (4), is also found to maximize the linear correlation coefficient indicating the consistency of our parameter estimation.

The high correlation indicates that our model is a good approximation of the underlying processes, although we have strongly simplified the real world. In particular, seasonal effects such as snow coverage are neglected. Additionally, the crust is assumed to be a homogeneous half-space which certainly is an oversimplified model of the local geology, where systems of open fractures are observed (*20*) extending from the surface to depth of at least 100m. Furthermore, we neglected the coseismic stress changes induced by the earthquakes themselves, which are known to trigger local aftershocks according to the Omori law (*21*).

Previous studies of natural swarm activity in the Vogtland region, Central Europe, indicate that aftershock sequences are embedded in the swarm activity and can even dominate it (*22*). However, for the Mt. Hochstaufen region, simple stacking of the activity relative to the largest events indicates that aftershocks play only a minor role.

The absolute pressure change due to rainfall depends only weakly on the value of the hydraulic diffusivity and is found to be between 0.005 - 0.013 bar in the depth range between 1-4 km, where most of the earthquakes occurred. This is in the same range as the effects of earth tides (*23*). However, inserting tidal stresses (calculated from volume strain at 2 km depth below Bad Reichenhall) as the loading mechanism into our model yields a maximum effect of only 15% compared to the rainfall induced rate changes. The relative effect of tides would be further reduced if one assumes that rain is collected in open fracture systems at the surface, which would enhance the rainfall induced effect.

Although some seasonal variability of seismicity related to ground water recharge and precipitation has been previously observed (*24*, *25*), we can show here for the first time a statistically significant causal relationship between rainfall and earthquake activity for an isolated region. Our analysis of the high quality meteorological and seismic data in the Mt. Hochstaufen region yields clear evidence

that tiny pore pressure changes induced by rainfall are able to trigger earthquake activity even at 4 km depth via the mechanism of fluid diffusion. Stress changes of the order of millibar are found to trigger earthquakes. This is much less than usually produced in fluid injection experiments (several 100 bars and more), indicating an extreme sensitivity of the crust with regard to minute changes. This might be an universal feature which can, however, only be seen in the rare occasion of an isolated but critical system. Although the reason for this criticality of the seismogenic volume in the Mt. Hochstaufen region is not yet resolved, the high correlation between rain-induced pressure changes at depth and seismicity opens the possibility of forecasting future earthquake rates on the basis of rainfall data in this region.

1. N. Sleep, M. L. Blanpied, *Nature* **359**, 687 (1992).
2. S. Kodaira, T. Idaka, A. Kato, J. Park, Y. Kaneda, *Science* **304**, 1295 (2004).
3. A. Nur, J. Booker, *Science* **175**, 885 (1972).
4. S. A. Miller *et al.*, *Nature* **427**, 724 (2004).
5. S. G. Prejean *et al.*, *Bull. Seism. Soc. Am.* **94**, 348 (2004).
6. P. Talwani, *Pure Appl. Geophys.* **150**, 473 (1997).
7. M. D. Zoback, H.-P. Harjes, *J. Geophys. Res.* **102**, 18,477 (1997).

8. J. H. Dieterich, *J. Geophys. Res.* **99**, 2601 (1994).

9. J. H. Dieterich, V. Cayol, P. Okubo, *Nature* **408**, 457 (2000).

10. H. Bögel, K. Schmidt, *Kleine Geologie der Ostalpen* (Ott Verlag Thun, Switzerland, 1976).

11. T. Kraft, J. Wassermann, E. Schmedes, H. Igel, submitted to *Tectonophysics* (December 2005).

12. T. Kraft, J. Wassermann, H. Igel, submitted to *Geophys. J. Int.* (March 2006).

13. M. Biot, *J. Appl. Phys.* **33**, 1482 (1962).

14. S. A. Shapiro, E. Huenges, G. Borm, *Geophys. J. Int.* **131**, F15 (1997).

15. D. Sornette, *Critical phenomena in natural sciences* (Springer-Verlag Berlin Heidelberg, 2000).

16. C. H. Scholz, *Nature* **391**, 37 (1998).

17. R. Harris, *J. Geophys. Res.* **103**, 24,347 (1998).

18. J. D. Byerlee, *Pure Appl. Geophys.* **116**, 615 (1978).

19. D. J. Daley, D. Vere-Jones, *An Introduction to the Theory of Point Processes, Volume I: Elementary Theory and Methods* (2nd ed., Springer, 2003).

20. M. Weede, *Die Geologie des Hochstaufen unter besonderer Berücksichtigung der Massenbewegungen* (Diploma Thesis, Technical University of Munich, 2002).

21. R. S. Stein, *Nature* **402**, 605 (1999).

22. S. Hainzl, Y. Ogata, *J. Geophys. Res.* **110**, B05S07, doi: 10.1029/2004JB003247 (2005).

23. M. Tolstoy, F. L. Vernon, J. A. Orcutt, F. K. Wyatt, *Geology* **30**, 503 (2002).

24. O. Saar, M. Manga, *Earth Planet. Sci. Lett.* **214**, 605 (2003).

25. B. Muco, *Phys. Earth Planet. Int.* **114**, 119 (1999).

Acknowledgments

The authors want to thank Jim Dieterich and Agnes Helmstetter for helpful discussion of the rate-state friction framework. Furthermore, we are thankful to Thomas Jahr for calculating the tidal effects and Ed Sobel for carefully reading the manuscript. This work was supported by the Deutsche Forschungsgemeinschaft (SCHE280/14-2 and 249351), Bavarian Ministry for Environment, and the EU Community initiative INTERREG III B Alpine Space Programme SISMOVALP.

Figure 1: Map of Staufen Massif as well as EW and NS profiles through the summit of Mt. Hochstaufen (1775m) with the located earthquakes in the year 2002 (red dots). Map borders are longitude $12^o40'$ - $12^o57'E$ and latitude $47^o40.5'$ - $47^o55.5'N$. Black triangles mark seismological stations installed in 2002.

Figure 2: The spatiotemporal pattern of (B) pore pressure and (C) estimated earthquake rate as the result of the surface rain rate (A) in the case of one-dimensional linear diffusion with hydraulic diffusivity D=2.9 m/s^2. Earthquake locations are marked by white stars (big: errors$\leq$100m). (D) shows the daily number of detected earthquakes (green) in comparison with the theoretical rate for the 1-4 km depth interval (red).

Figure 3: The linear correlation coefficient as a function of the time shift between the time series of the daily observed number of earthquakes and (i) the daily rain amount (dashed line) and (ii) the theoretical rate of earthquakes in the 1-4 km depth interval (solid line).

Figure 1:

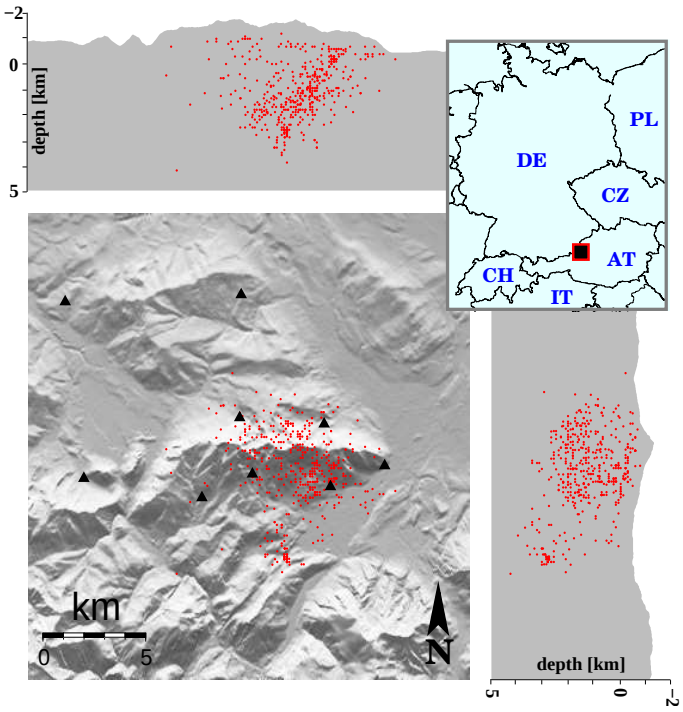

Figure 2:

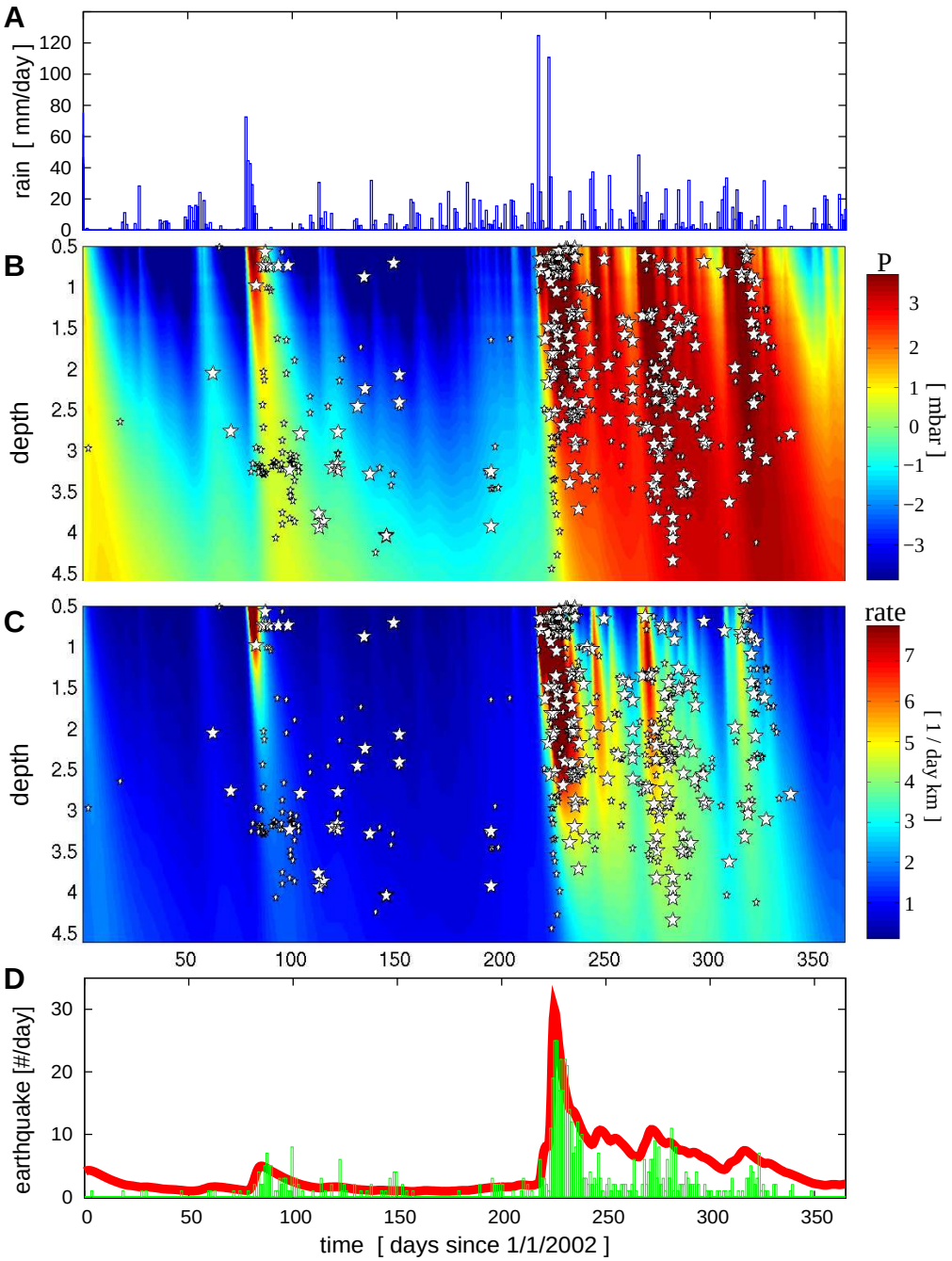
A
rain [mm/day]
0
20
40
60
80
100
120
B
depth
0.5
1
1.5
2
2.5
3
3.5
4
4.5
P
[mbar]
3
2
1
0
−1
−2
−3
C
depth
rate
[1 / day km]
7
6
5
4
3
2
1
50
100
150
200
250
300
350
D
earthquake [#/day]
0
10
20
30
time [days since 1/1/2002]

Figure 3:

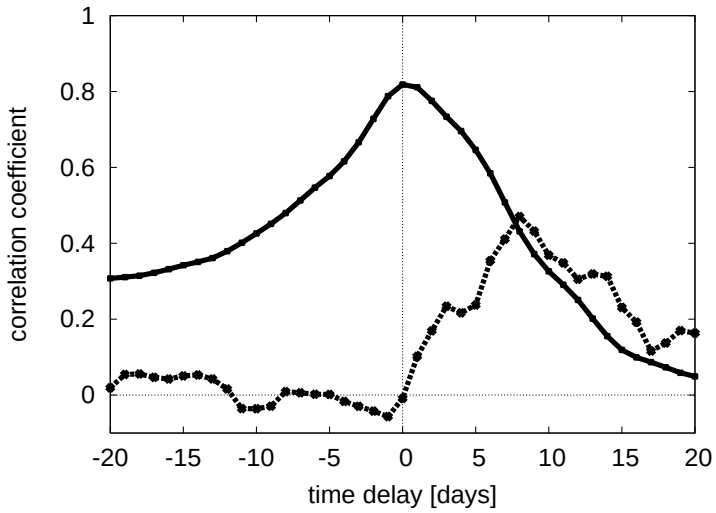
correlation coefficient
1
0.8
0.6
0.4
0.2
0
-20
-15
-10
-5
0
5
10
15
20
time delay [days]